

Phase transition-induced superstructures of *β*-Sn films with atomic-scale thickness

Le Lei(雷乐), Feiyue Cao(曹飞跃), Shuya Xing(邢淑雅), Haoyu Dong(董皓宇), Jianfeng Guo(郭剑锋), Shangzhi Gu(顾尚志), Yanyan Geng(耿燕燕), Shuo Mi(米烁), Hanxiang Wu(吴翰翔), Fei Pang(庞斐), Rui Xu(许瑞), Wei Ji(季威), and Zhihai Cheng(程志海)

Citation: Chin. Phys. B, 2021, 30 (**9**): 096804. DOI: 10.1088/1674-1056/ac11e8
Journal homepage: http://cpb.iphy.ac.cn; http://iopscience.iop.org/cpb

What follows is a list of articles you may be interested in

Epitaxial growth of antimony nanofilms on HOPG and thermal desorption to control the film thickness

Shuya Xing(邢淑雅), Le Lei(雷乐), Haoyu Dong(董皓宇), Jianfeng Guo(郭剑峰), Feiyue Cao(曹飞跃), Shangzhi Gu(顾尚志), Sabir Hussain, Fei Pang(庞斐), Wei Ji(季威), Rui Xu(许瑞), Zhihai Cheng(程志海)
Chin. Phys. B, 2020, 29 (**9**): 096801. DOI: 10.1088/1674-1056/aba27c

STM study of selenium adsorption on Au(111) surface

Bin Liu(刘斌), Yuan Zhuang(庄源), Yande Que(阙炎德), Chaoqiang Xu(徐超强), Xudong Xiao(肖旭东)
Chin. Phys. B, 2020, 29 (**5**): 056801. DOI: 10.1088/1674-1056/ab821d

High quality $PdTe_2$ thin films grown by molecular beam epitaxy

En Li(李恩), Rui-Zi Zhang(张瑞梓), Hang Li(李航), Chen Liu(刘晨), Geng Li(李更), Jia-Ou Wang(王嘉鸥), Tian Qian(钱天), Hong Ding(丁洪), Yu-Yang Zhang(张余洋), Shi-Xuan Du(杜世萱), Xiao Lin(林晓), Hong-Jun Gao(高鸿钧)
Chin. Phys. B, 2018, 27 (**8**): 086804. DOI: 10.1088/1674-1056/27/8/086804

Fabrication and properties of silicene and silicene–graphene layered structures on Ir (111)

Meng Lei, Wang Ye-Liang, Zhang Li-Zhi, Du Shi-Xuan, Gao Hong-Jun
Chin. Phys. B, 2015, 24 (**8**): 086803. DOI: 10.1088/1674-1056/24/8/086803

Structural and physical properties of $BiFeO_3$ thin films epitaxially grown on $SrTiO_3$ (001) and polar (111) surfaces

He Shu-Min, Liu Guo-Lei, Zhu Da-Peng, Kang Shi-Shou, Chen Yan-Xue, Yan Shi-Shen, Mei Liang-Mo
Chin. Phys. B, 2014, 23 (**3**): 036801. DOI: 10.1088/1674-1056/23/3/036801

Phase transition-induced superstructures of β-Sn films with atomic-scale thickness*

Le Lei(雷乐), Feiyue Cao(曹飞跃), Shuya Xing(邢淑雅), Haoyu Dong(董皓宇), Jianfeng Guo(郭剑锋), Shangzhi Gu(顾尚志), Yanyan Geng(耿燕燕), Shuo Mi(米烁), Hanxiang Wu(吴翰翔), Fei Pang(庞斐), Rui Xu(许瑞), Wei Ji(季威), and Zhihai Cheng(程志海)†

Beijing Key Laboratory of Optoelectronic Functional Materials & Micro-nano Devices, Department of Physics, Renmin University of China, Beijing 100872, *China*

(Received 13 May 2021; revised manuscript received 9 June 2021; accepted manuscript online 7 July 2021)

The ultrathin β-Sn(001) films have attracted tremendous attention owing to its topological superconductivity (TSC), which hosts Majorana bound state (MBSs) for quantum computation. Recently, β-Sn(001) thin films have been successfully fabricated via phase transition engineering. However, the understanding of structural phase transition of β-Sn(001) thin films is still elusive. Here, we report the direct growth of ultrathin β-Sn(001) films epitaxially on the highly oriented pyrolytic graphite (HOPG) substrate and the characterization of intricate structural-transition-induced superstructures. The morphology was obtained by using atomic force microscopy (AFM) and low-temperature scanning tunneling microscopy (STM), indicating a structure-related bilayer-by-bilayer growth mode. The ultrathin β-Sn film was made of multiple domains with various superstructures. Both high-symmetric and distorted superstructures were observed in the atomic-resolution STM images of these domains. The formation mechanism of these superstructures was further discussed based on the structural phase transition of β to α-Sn at the atomic-scale thickness. Our work not only brings a deep understanding of the structural phase transition of Sn film at the two-dimensional limit, but also paves a way to investigate their structure-sensitive topological properties.

Keywords: epitaxial growth, β-Sn films, bilayer-by-bilayer, superstructures, structural transition, scanning tunneling microscopy, surface energy

PACS: 68.37.−d, 68.55.−a, 68.37.Ef, 68.65.Cd **DOI:** 10.1088/1674-1056/ac11e8

1. Introduction

Since the discovery and characterization of graphene,[1,2] the novel two-dimensional (2D) materials, especially for monoelemental 2D materials, have been the subject of an increasing area of research due to their exotic non-trivial topological properties and potential applications.[3–10] In the periodic table, most of 2D monoelemental materials, consisting of the elements in the main group of IIIA, IVA, and VA, have been successfully prepared, such as borophene,[11–14] silicene,[15–17] antimonene,[18–21] bismuthine,[5,22,23] and so on.[24–26] Among them, the 2D materials consisted of heavy elements have been predicted as topological insulators with enhanced bulk gap and nontrivial edge state due to their strong spin–orbit coupling (SOC).[27–29] For instance, the bismuthine grown on SiC(0001) substrate shows a large gap of ~ 0.8 eV and conductive edge states.[23] The ultraflat stanene on Cu(111) exhibits a topological bandgap (~ 0.3 eV) induced by SOC at the Γ point.[30] The robust one-dimensional topological edge state of antimonene monolayer has been also observed experimentally.[31]

It is well known that bulk Sn exhibits two kinds of phases.[32] The one is semiconducting α-Sn with diamond structure at low temperature, while the other one is metallic β-Sn at high temperature, which has a body-centered tetragonal (bct) structure. The bulk Sn undergoes a phase transition from β-Sn to α-Sn at 285 K upon cooling process.[33] The monolayer α-Sn(111) with honeycomb structure, known as stanene, has been theoretically predicted to be a topological insulator with nontrivial edge states.[28,34] The stanene has been further successfully prepared by molecular beam epitaxy (MBE).[30,35] In recent years, the search for Majorana bound states (MBSs) in condensed matter systems has attracted a great deal of interests for potential applications in topological quantum computing.[36–40] The bulk β-Sn is a typical superconductor below 3.72 K.[41] The further theoretical exploration points out that the ultrathin β-Sn(001) is an ideal platform for topological superconductor (TSC) with MBSs.[42] Recently, the strained β-Sn(001) thin films were obtained via phase transition engineering by leaving the fcc-Sn (111) at room temperature for some weeks.[43] The α-Sn thin films can also transform into strained β-Sn films with the increase of thickness because of the large lattice mismatch and symmetry

*Project supported by the National Natural Science Foundation of China (Grant Nos. 61674045, 61911540074, and 21622304), the Fund from the Ministry of Science and Technology of China (Grant No. 2016YFA0200700), the Strategic Priority Research Program and Key Research Program of Frontier Sciences (Chinese Academy of Sciences) (Grant Nos. XDB30000000 and QYZDB-SSW-SYS031). Zhihai Cheng was supported by the Fundamental Research Funds for the Central Universities and the Research Funds of Renmin University of China (Grant No. 21XNLG27).

†Corresponding author. E-mail: zhihaicheng@ruc.edu.cn

© 2021 Chinese Physical Society and IOP Publishing Ltd

difference.[32,44] The one-step growth and the detailed structural characterization of ultrathin β-Sn films are still lacking.

In this work, we successfully synthesize the large-scale ultrathin β-Sn(001) films on highly oriented pyrolytic graphite (HOPG) substrate by using MBE and a series of complex superstructures were systematically characterized by atomic force microscopy (AFM) and scanning tunneling microscopy (STM). The measurement of step height of Sn films reveals the bilayer-by-bilayer growth mode. The high-resolution STM images found that ultrathin β-Sn(001) film was composed of numerous domains with various superstructures. The atomic-resolution STM images further indicate that some domains present high-symmetric superstructures, including $\sqrt{2}\times\sqrt{2}$, 5×5, and $3\sqrt{2}\times3\sqrt{2}$ superlattices, and other domains show distorted superstructures. The formation mechanism of superstructures in domains was also discussed based on the structural phase transition of β- to α-Sn at the atomic-scale thickness. Our finding provides new insight into understanding the structural phase transition of Sn film and opens opportunities for exploring topological properties and device applications.

2. Materials and methods

The sample preparation and STM/AFM measurements are described below. The β-Sn thin film was grown on freshly cleaved highly oriented pyrolytic graphite (HOPG) substrates by standard MBE in ultra-high vacuum (UHV) chamber under a base pressure of 3.0×10^{-10} Torr (1 Torr $=1.33322\times10^{2}$ Pa). The HOPG substrate was cleaved in air and immediately loaded into the MBE chamber, then annealed at 773 K overnight to remove contaminants. High purity Sn (99.999%) was evaporated from the Knudsen cell onto the HOPG kept at $\sim$ 500 K. After the growth experiment, the sample was first transferred to another UHV chamber with LT-STM (PanScan Freedom, RHK) for the following STM measurements. The low temperature STM measurements were performed at 9 K with chemical etched W tip calibrated on a clean Au(111) surface. All STM images were processed by Gwyddion and WSxM software.[45] The AFM measurements were performed on a commercial AFM system (MFP-3D Infinity, Asylum Research), in combination with a dynamic signal analyzer (HF2LI, Zurich Instruments) in the atmosphere circumstance.

3. Results and discussion

Bulk Sn is allotropic with two stable phases of white β-Sn and gray α-Sn, and undergoes the structural phase transition at 286 K. The bulk β-Sn has a body-centered tetragonal (bct) structure (A5, space group $I4/amd$) with lattice constants of $a=5.82$ Å and $c=3.18$ Å, as shown in Fig. 1(a). Figure 1(c) illustrates the diamond crystal structure of bulk α-Sn ($a=6.49$ Å, space group $Fd3m$). Figure 1(b) shows the bilayer structural model of β-Sn with double unit cells. The number 8 of Sn atoms in a unit cell of α-Sn is identical with that of double unit cells of β-Sn, which could play important roles in the structural phase transition of α-β Sn. In bulk Sn, this phase transition is well known as tin pest[46] due to the powdering of α-Sn from β-Sn when cooling. The volume of α-Sn (273 Å^3/unit cell) is pronouncedly larger than that of β-Sn (216 Å^3/double unit cell), which results in a $\sim$ 26% volume increase of phase transition from β-Sn to α-Sn. The bulk Sn occurred during phase transition is so structurally weak that readily crumbles into powder due to huge internal compressive strain. While the structural phase transition behavior of Sn films with atomic-scale thickness is still not clear, which may play important roles in determining their morphology, structures and properties significantly.

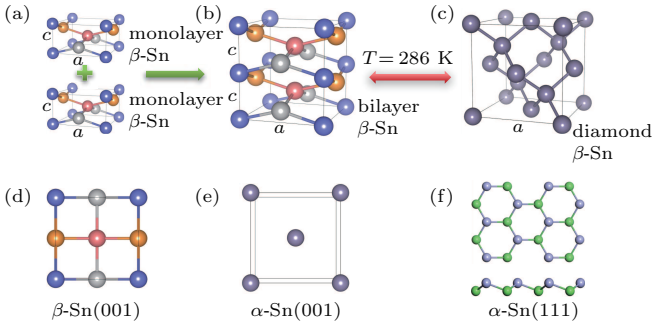


Fig. 1. Atomic structural models and phase transition of Sn. (a) and (b) Atomic structural models of monolayer (a) and bilayer (b) β-Sn (bct structure, white tin), respectively. (c) Atomic structural models of α-Sn (diamond structure, grey tin). (d) Top view of atomic structure of β-Sn(001) surface. (e) Top view of atomic structure of α-Sn(001) surface. (f) Top view (upper) and side view (lower) of atomic structure of α-Sn(111) surface. Bulk tin undergoes a structural phase transition of α-Sn to β-Sn at $\sim$ 286 K.

As we know, the Sn belongs to the elements of group IVA in the periodic table. Among of the elements of group IVA, C, Si, and Ge exhibit strong semiconducting property due to they have a tendency to form covalent diamond structure by strong sp^3 hybridization at ambient conditions.[47] The sp^3 hybridization becomes weaker as the atomic number increases in the elements of group IVA. The heavy element Pb shows a metallic fcc structure due to the prohibition of formation of sp^3 bonds. The position of Sn in the elements of group IVA is the borderline between light elements (C, Si, and Ge) and heavy element (Pb). Therefore, the covalent diamond structure of α-Sn is relatively weak at low temperature[48] with zero-gap semiconducting property. The β-Sn is stable and metallic at high temperature due to the metallic bonding nature in body-centered tetragonal crystal structure.

For ultrathin Sn film, it is clear that the surface structure and stability of ultrathin Sn film will pronouncedly affect the structural phase transition behaviors. The (001) surfaces of β-Sn films and α-Sn films are relatively stable with similar fourfold symmetric structure, as shown in Figs. 1(d) and 1(e). The surface atoms of α-Sn(001) surface is flat and more close-packed than that of β-Sn films. Therefore, it can be speculated

that the β-Sn(001) surface has a tendency to transform into α-Sn(001) surface by the upward moving of central pink Sn atom to reduce the surface corrugation and surface energy. The β-Sn(001) surface of Sn films still have a tendency to further transform into the most stable and close-packed (111) surface of α-Sn films with threefold symmetric structure. It is clear that the above surface transformation will introduce significantly interval in-plane compressive strain within the ultra Sn films, which may affect their surface morphology and lattice structures.

The high-quality β-Sn films were successfully synthesized on HOPG, and further characterized by AFM and STM. Figure 2(a) shows a large-scale AFM topography images of the as-prepared Sn films with lateral sizes of $\sim$ 600 nm–800 nm. It seems that the Sn nanofilms were made of many merged small islands and represent a multi-domain crystalized structure. Figure 2(b) shows the typical large-scale STM topographic image of Sn nanofilms, in which the merged small islands with uniform thickness are clearly resolved in the Frankvan der Verwe (layer-by-layer) growth mode.

Figure 2(c) shows the high-resolution STM image of Sn films with many step edges. The surface of Sn films was smooth and flat, suggesting their high crystallinity. Unexpectedly, all the step heights of Sn films are $\sim$ 0.6 nm, as shown in Fig. 2(d), which is consistent with the bilayer height of β-Sn films. More line profiles are supplied in Fig. S1 to indicate the exclusive step heights of bilayer. As shown in Figs. 1(b) and 1(c), the bilayer-by-bilayer growth mode of Sn films at here should be related with the similarity of unit cell for the α-Sn monolayer and β-Sn bilayer during the structural transition of β-Sn to α-Sn.

The multi-domain structures of Sn nanofilms were further clearly resolved, as shown in the STM topography and corresponding current images of Figs. 2(e) and 2(f). The various domains were only vaguely observed in the topographic images due to their very small apparent height difference, while can be clearly resolved in the current images via their different long-range ordered surface structures. The apparent height difference between the domains is far less than the thickness ($\sim$ 0.32 nm) of monolayer β-Sn(001) monolayer, as shown in Figs. 2(g) and 2(h). More STM images of Sn nanofilms with multi structural domains were supplied in Fig. S2.

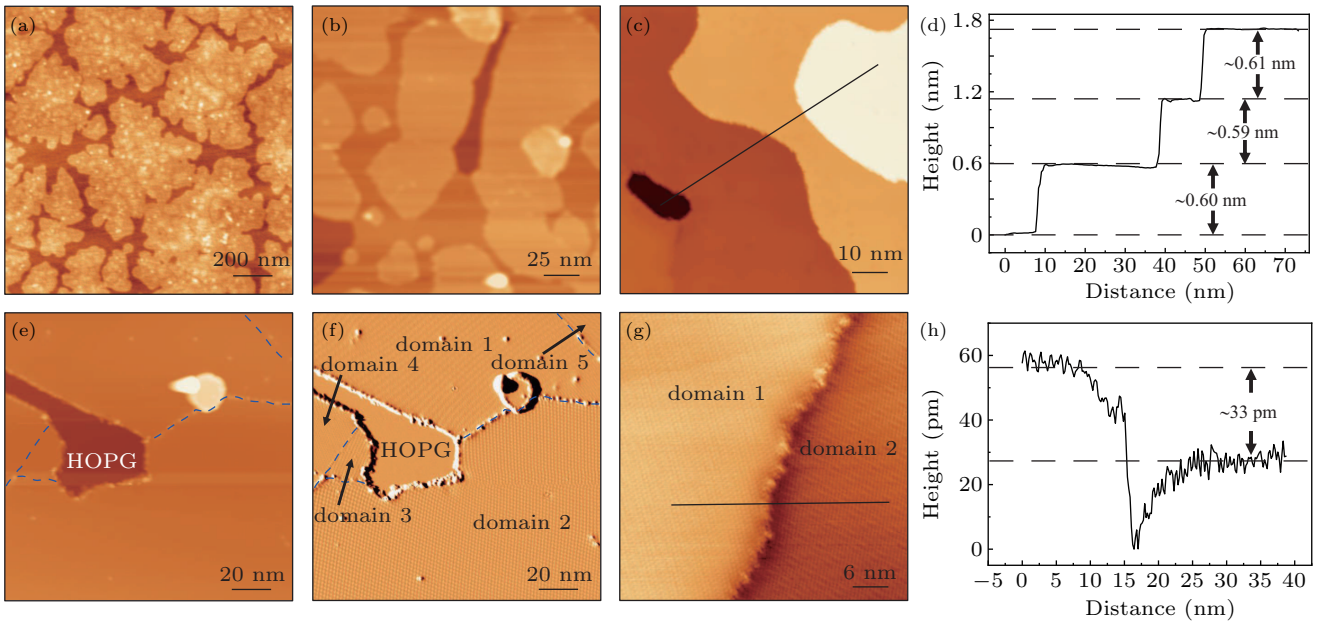


Fig. 2. Epitaxially growth of the β-Sn films on HOPG substrate. (a) AFM morphology image of Sn films. (b) Large-scale STM topographic image of Sn films. (c) High-resolution STM topographic image of the Sn films. (d) Line profile taken along the black line in panel (c). The bilayer-by-bilayer growth mode of Sn films is confirmed by the step heights of $\sim$ 0.6 nm. (e) and (f) STM topography (e) and corresponding current (f) images of Sn films. The various structural domains were clearly resolved within the Sn films and highlighted with the domain walls marked by blue dashed lines. (g) High-resolution STM image with domains. (h) Line profile taken along the black line in panel (g). The small topography difference is observed between different domains of Sn films. (b) $V = 1.6$ V, $I = 200$ pA; (c): $V = -2.4$ V, $I = -300$ pA; (e)–(f): $V = 1.8$ V, $I = 100$ pA; (g): $V = -0.8$ V, $I = -200$ pA.

The high-symmetric superstructures of the domains within the β-Sn films were first carefully investigated via the high-resolution STM images. Figure 3(a) shows the atomically resolved STM image of the domain with the flat surface atoms and smallest (1×1) square lattice. The corresponding unit cell (marked with red solid square) is measured to be 0.41 nm $\times$0.41 nm, which is not consistent with the pristine surface structure of β-Sn(001) in Fig. 1(d). If the central pink Sn atoms of β-Sn(001) move upward to form the flat and close-packed (001) surface to reduce the surface energy, the arrangement of surface Sn atoms in the surface will be almost identical with those in Fig. 3(a), as shown by the schematic modes of Fig. 3(i). Actually, this unique flat surface structure in Fig. 3(a) is very similar to the α-Sn(001) surface in Fig. 1(f),

which can be speculated as the surface transition of β-Sn to α-Sn film at the earliest stage. It is clear that the significant compressive in-plane strain was introduced into the Sn nanofilms during the above surface transition. The pristine surface structure of β-Sn(001) (called $\sqrt{2}\times\sqrt{2}$ superstructure here) was rarely observed, as shown in Fig. 3(b), which seems unstable and is difficult to be imaged in the STM measurements.

The high-symmetric superstructures with larger lattices of 5×5 and $3\sqrt{2}\times3\sqrt{2}$ were also observed on the surfaces of other domains, as shown in Figs. 3(c) and 3(d). The corresponding structural models were schematically shown in Fig. 3(i). It is noted that the four-fold symmetry is still preserved, while the translation symmetry is reduced due to the formation of larger square supercells. Then, these superstructures can be speculated as the further tentative transition from α-Sn to β-Sn nanofilms after the above surface transition. The larger supercells can not only decrease the transition barriers of internal Sn atoms but also reduced the in-pane compressive strain energy via the surface corrugations in comparison with the atomic flat surface of Fig. 3(a). The similar supercell sizes of 5×5 and $3\sqrt{2}\times3\sqrt{2}$ in the β-Sn bilayer nanofilms suggest that the volume of ~1.2 nm^3 (~72 atoms) should be the critical size for the relaxation of Sn atoms during the phase transition process.

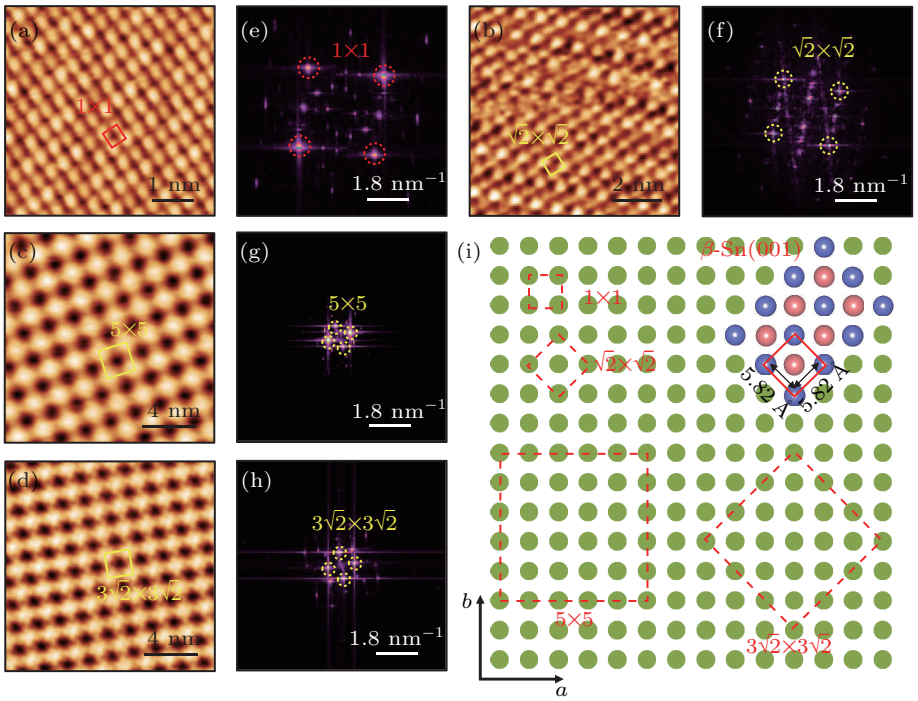


Fig. 3. High-symmetric superstructures of the domains within the β-Sn nanofilms on HOPG substrate. (a)–(d) Atomic-resolution STM images of the β-Sn domains. The unit cells are marked with red and yellow solid squares. (e)–(h) The corresponding FFT images of panels (a)–(d), respectively. (i) Schematic models of the observed surface superstructures. The green spheres represent the surface Sn atoms, and the theoretical atomic structure of β-Sn(001) surface is shown at the top right corner. (a) $V=1.7$ V, $I=200$ pA; (b) $V=0.6$ V, $I=200$ pA; (c) $V=2.7$ V, $I=50$ pA; (d) $V=2.5$ V, $I=100$ pA.

In addition to the above two high-symmetric superstructures, most of the domains within the β-Sn nanofilms show various distorted superstructures with parallelograms superlattice. These distorted superstructures could be speculated as the further transformation to the close-packed (111) surface of α-Sn film with threefold symmetry. Figures 4(a) and 4(b) show two typical of distorted superstructures with different parallelogram superlattices. The superstructures in Figs. 4(a) and 4(b) can be assumed as the distorted forms from the high-symmetric 3×4 and $2\sqrt{2}\times3\sqrt{2}$ superstructures. The primitive vectors of these distorted superstructure are closed to the directions of the 1×1 or $\sqrt{2}\times\sqrt{2}$ lattice with the intersection angle of $\sim60^\circ$. Figure S3 shows the STM images of other distorted superstructures with more complicated super lattices. Figure 4(c) shows another kind of striped superstructure with the high-symmetric $\sqrt{3}\times3\sqrt{2}$ superlattice and larger surface corrugations. One of its primitive vectors is incommensurate with the $\sqrt{2}\times\sqrt{2}$ lattice of β-Sn(001) surface. It is clearly that the striped superstructures can also reduce the internal strain energy of structural transition, while its detailed formation mechanism is still not clear.

Finally, the bilayerbybilayer growth mode and various superstructures of the epitaxial β-Sn films are phenomenally discussed based on the structural transition of β-Sn to α-Sn at the two-dimensional limit. Firstly, the tentative structural transitions of β-Sn to α-Sn films adopt the whole bilayer transform due to their identical number of Sn atoms, as shown in Figs. 1(b) and 1(c). Secondly, the first step of structural transition is the surface transformation of β-Sn(001) to α-Sn(001) by moving the central Sn atom upward to get the flat surface and reduce surface energy. In this step, the (001) surface of the β-Sn films provides the most convenient relax-

ation mechanism for the structural transition, while the fourfold symmetry and size of the surface unit cell are still preserved. Thirdly, the high-symmetric superstructures with large square unit cells were formed with large surface corrugations (as shown in Fig. S5) to release the significant internal compressive strain during the further structural transition. In this step, the fourfold symmetry of the Sn films is still preserved, while the translation symmetry is reduced with large supercells of similar size. Fourthly, the above fourfold-symmetric superstructures were further distorted to tentatively transform into the most stable and close-packed α-Sn(111) surface with threefold symmetry. In a word, the epitaxial growth of ultrathin β-Sn films is realized on the inert HOPG substrate. The Sn films stay long enough at room temperature and low temperature. However, the complete transition from β- to α-Sn was not observed. The β-Sn films have a trend to transform into α-Sn films at low temperature. The unique arrangement of surface Sn atoms in the surface and multiple superstructures observed in our experiments were introduced due to the structural phase transition trend from β-Sn to α-Sn films at low temperature at the two-dimensional limit.

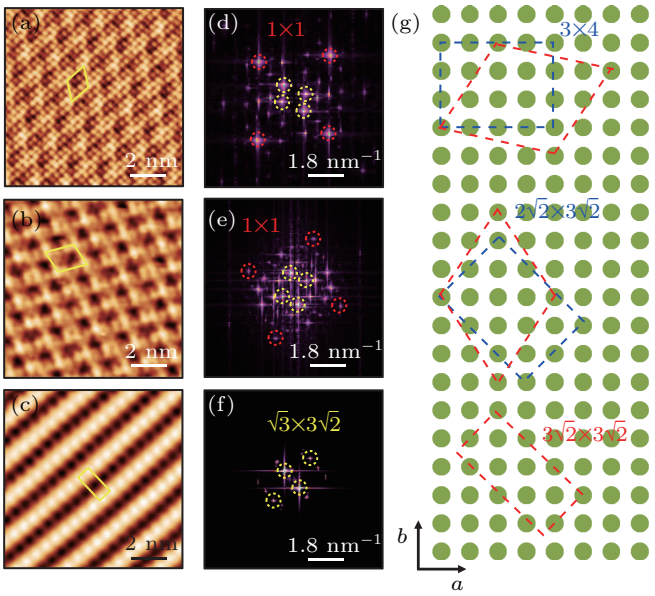


Fig. 4. Distorted superstructures of the domains within the β-Sn films on HOPG substrate. (a) and (b) High resolution STM topography images of two distorted superstructures with parallelograms superlattice. The super cells are marked with the yellow solid parallelograms. (c) High-resolution STM image of striped superstructure with rectangular superlattice marked by the yellow solid rectangle. (d)–(f) The corresponding FFT images of panels (a)–(c), respectively. (g) Schematic illustrations of distorted [(a) and (b)] and striped (c) superstructures. The red dashed parallelograms represent distorted superstructures from the superstructures with rectangular superlattice marked by the blue-dashed rectangles. (a) $V = 2.2$ V, $I = 100$ pA; (b) $V = 0.4$ V, $I = 300$ pA; (c) $V = 1.9$ V, $I = 200$ pA.

The electronic properties of the Sn films were further investigated by the scanning tunneling spectroscopy (STS) measurement. The similar $\mathrm{d}I/\mathrm{d}V$ spectra taken at various structural domains is shown in Fig. S4 with finite local density of states (LDOS) at the Fermi energy (E_F), indicating the metallic property of the Sn films. This result is consistent with the band structure of the β-Sn films calculated by density functional theory (DFT).[42] The ultrathin Sn films with various superstructures could exhibit interesting modified superconductive and topological properties, which will inspire more experimental and theoretical work on this idea platform for topological superconductivity.

4. Conclusion

In summary, we have successfully grown ultrathin β-Sn (001) films on HOPG substrates and systematically explored various superstructures observed in ultrathin β-Sn (001) films. We confirm that β-Sn (001) films growth with a bilayer-by-bilayer growth mode. The further study found that there are various domains in the β-Sn (001) films. The long-range ordered superstructures in different domains, including high-symmetric and distorted superstructures, were systematically characterized. We assume that these superstructures are induced via structural phase transition of β- to α-Sn at the two-dimensional limit. Our study not only demonstrates the importance of the structural phase transition during the formation of superstructures of β-Sn, but also opens a door for studying topological properties of β-Sn thin films in the future.

References

[1] Novoselov K S, Geim A K, Morozov S V, Jiang D, Zhang Y, Dubonos S V, Grigorieva I V and Firsov A A 2004 *Science* **306** 666
[2] Zhang Y, Tan Y W, Stormer H L and Kim P 2005 *Nature* **438** 201
[3] Liao M, Zang Y, Guan Z, Li H, Gong Y, Zhu K, Hu X P, Zhang D, Xu Y, Wang Y Y, He K, Ma X C, Zhang S C and Xue Q K 2018 *Nat. Phys.* **14** 344
[4] Falson J, Xu Y, Liao M, Zang Y, Zhu K, Wang C, Zhang Z, Liu H, Duan W, He K, Liu H, Smet J H, Zhang D and Xue Q K 2020 *Science* **367** 1454
[5] Stühler R, Reis F, Müller T, Helbig T, Schwemmer T, Thomale R, Schäfer J and Claessen R 2020 *Nat. Phys.* **16** 47
[6] Ling Z B, Zhang Q Y, Yang C P, Li X T, Liang W S, Wang Y Q, Yang H W and Sun J R 2020 *Chin. Phys. B* **29** 096802
[7] Sun Q L, Wang L, Wang W Q, Sun L, Li M C, Wang W X, Jia H Q, Zhou J M and Chen H 2015 *Chin. Phys. Lett.* **32** 106801
[8] Fakir M S, Ahmad Z and Sulaiman K 2012 *Chin. Phys. Lett.* **29** 126802
[9] Dong J and Ouyang G 2020 *Chin. Phys. B* **29** 086403
[10] Ding C, Liu C, Zhang Q H, Gong G M, Wang H, Liu X Z, Meng F Q, Yang H H, Wu R, Song C L, Li W, He K, Ma X C, Gu L, Wang L L and Xue Q K 2018 *Acta Phys. Sin.* **67** 207415 (in Chinese)
[11] Feng B, Zhang J, Zhong Q, Li W, Li S, Li H, Cheng P, Meng S, Chen L and Wu K 2016 *Nat. Chem.* **8** 563
[12] Mannix A J, Zhou X F, Kiraly B, Wood J D, Alducin D, Myers B D, Liu X, Fisher B L, Santiago U, Guest J R, Yacaman M J, Ponce A, Oganov A R, Hersam M C and Guisinger N P 2015 *Science* **350** 1513
[13] Wu R, Drozdov I K, Eltinge S, Zahl P, Ismail-Beigi S, Bozovic I and Gozar A 2019 *Nat. Nanotechnol.* **14** 44
[14] Zhong Q, Kong L, Gou J, Li W, Sheng S, Yang S, Cheng P, Li H, Wu K and Chen L 2017 *Phys. Rev. Mater.* **1** 021001
[15] Meng L, Wang Y, Zhang L, Du S, Wu R, Li L, Zhang Y, Li G, Zhou H, Hofer W A and Gao H J 2013 *Nano Lett.* **13** 685
[16] Feng B, Ding Z, Meng S, Yao Y, He X, Cheng P, Chen L and Wu K 2012 *Nano Lett.* **12** 3507
[17] Chen L, Liu C C, Feng B, He X, Cheng P, Ding Z, Meng S, Yao Y and Wu K 2012 *Phys. Rev. Lett.* **109** 056804
[18] Shao Y, Liu Z L, Cheng C, Wu X, Liu H, Liu C, Wang J O, Zhu S Y, Wang Y Q, Shi D X, Ibrahim K, Sun J T, Wang Y L and Gao H J 2018 *Nano Lett.* **18** 2133

[19] Shi Z Q, Li H, Xue C L, Yuan Q Q, Lv Y Y, Xu Y J, Jia Z Y, Gao L, Chen Y, Zhu W and Li S C 2020 *Nano Lett.* **20** 8408

[20] Shi Z Q, Li H, Yuan Q Q, Song Y H, Lv Y Y, Shi W, Jia Z Y, Gao L, Chen Y B, Zhu W and Li S C 2019 *Adv. Mater.* **31** 1806130

[21] Xing S, Lei L, Dong H, Guo J, Cao F, Gu S, Hussain S, Pang F, Ji W, Xu R and Cheng Z 2020 *Chin. Phys. B* **29** 096801

[22] Reis F, Li G, Dudy L, Bauernfeind M, Glass S, Hanke W, Thomale R, Schafer J and Claessen R 2017 *Science* **357** 287

[23] Du H, Sun X, Liu X, Wu X, Wang J, Tian M, Zhao A, Luo Y, Yang J, Wang B and Hou J G 2016 *Nat. Commun.* **7** 10814

[24] Xu J P, Zhang J Q, Tian H, Xu H, Ho W and Xie M 2017 *Phys. Rev. Mater.* **1** 061002

[25] Zhou D, Meng Q, Si N, Zhou X, Zhai S, Tang Q, Ji Q, Zhou M, Niu T and Fuchs H 2020 *ACS Nano* **14** 2385

[26] Zhang Z M, Zhang W H and Fu Y S 2019 *Acta Phys. Sin.* **68** 226801 (in Chinese)

[27] Liu C C, Feng W and Yao Y 2011 *Phys. Rev. Lett.* **107** 076802

[28] Xu Y, Yan B, Zhang H J, Wang J, Xu G, Tang P, Duan W and Zhang S C 2013 *Phys. Rev. Lett.* **111** 136804

[29] Kane C L and Mele E J 2005 *Phys. Rev. Lett.* **95** 226801

[30] Deng J, Xia B, Ma X, Chen H, Shan H, Zhai X, Li B, Zhao A, Xu Y, Duan W, Zhang S C, Wang B and Hou J G 2018 *Nat. Mater.* **17** 1081

[31] Zhu S Y, Shao Y, Wang E, Cao L, Li X Y, Liu Z L, Liu C, Liu L W, Wang J O, Ibrahim K, Sun J T, Wang Y L, Du S and Gao H J 2019 *Nano Lett.* **19** 6323

[32] Roldan Cuenya B, Doi M and Keune W 2002 *Surf. Sci.* **506** 33

[33] Wang D T, Esser N, Cardona M and Zegenhagen J 1995 *Surf. Sci.* **343** 31

[34] Xu Y, Tang P and Zhang S C 2015 *Phys. Rev. B* **92** 081112

[35] Zhu F F, Chen W J, Xu Y, Gao C L, Guan D D, Liu C H, Qian D, Zhang S C and Jia J F 2015 *Nat. Mater.* **14** 1020

[36] Wang D, Kong L, Fan P, Chen H, Zhu S, Liu W, Cao L, Sun Y, Du S, Schneeloch J, Zhong R, Gu G, Fu L, Ding H and Gao H J 2018 *Science* **362** 333

[37] Yuan Y, Pan J, Wang X, Fang Y, Song C, Wang L, He K, Ma X, Zhang H, Huang F, Li W and Xue Q K 2019 *Nat. Phys.* **15** 1046

[38] Wang Z, Rodriguez J O, Jiao L, Howard S, Graham M, Gu G D, Hughes T L, Morr D K and Madhavan V 2020 *Science* **367** 104

[39] Machida T, Sun Y, Pyon S, Takeda S, Kohsaka Y, Hanaguri T, Sasagawa T and Tamegai T 2019 *Nat. Mater.* **18** 811

[40] Gu Q Q, Wan S Y, Yang H and Wen H H 2018 *Acta Phys. Sin.* **67** 207401 (in Chinese)

[41] Eisenstein J 1954 *Rev. Mod. Phys.* **26** 277

[42] Lei C, Chen H and MacDonald A H 2018 *Phys. Rev. Lett.* **121** 227701

[43] Li AM, Lu D, Yang X Y, Zhu Z, Wang G Y, Guan D D, Zheng H, Li Y Y, Liu C, Qian D and Jia J F 2018 *Chin. Phys. Lett.* **35** 066802

[44] Wang L L, Ma X C, Ji S H, Fu Y S, Shen Q T, Jia J F, Kelly K F and Xue Q K 2008 *Phys. Rev. B* **77** 205410

[45] Horcas I, Fernandez R, Gomez-Rodriguez J M, Colchero J, Gomez-Herrero J and Baro A M 2007 *Rev. Sci. Instrum.* **78** 013705

[46] Cornelius B, Treivish S, Rosenthal Y and Pecht M 2017 *Microelectronics Reliability* **79** 175

[47] Mujica A, Rubio A, Munoz A and Needs R J 2003 *Rev. Mod. Phys.* **75** 863

[48] Christensen N E and Methfessel M 1993 *Phys. Rev. B* **48** 5797